Primary productivity in the central equatorial Pacific (3°S 130°W) during GasEx-2001

Peter G. Strutton[1]
Marine Sciences Research Center, State University of New York at Stony Brook, Stony Brook, New York, USA

Francisco P. Chavez
Monterey Bay Aquarium Research Institute, Moss Landing, California, USA

Richard C. Dugdale and Victoria Hogue
Romberg Tiburon Center, San Francisco State University, Tiburon, California, USA

Received 17 January 2003; revised 8 April 2004; accepted 14 May 2004; published 22 July 2004.

[1] Measurements of chlorophyll concentration, phytoplankton productivity, and nutrient dynamics were made during the GasEx-2001 cruise to the equatorial Pacific in February 2001. During the core measurement period of the experiment, a parcel of water was tracked over a 16-day period in order to close the mixed layer carbon budget. Chlorophyll concentration averaged 0.16 mg m^{-3} and integrated mixed layer primary productivity increased from 10 to 50 mmolC m^{-2} d^{-1}, concomitant with a shoaling of the thermocline. The mean *f* ratio (ratio of new to primary production) decreased from 0.17 at the surface to 0.04 at 60 m, and the ratio of silicate to nitrate uptake by phytoplankton was 0.8. These results are close to or slightly lower than climatological values, and are consistent with moderate productivity in an iron-silicate co-limited environment. Fast repetition rate (FRR) fluorometry indicated that the effects of iron limitation increased with distance from the equator, the origin of upwelled iron. Measured chlorophyll concentrations were used to calculate the attenuation of solar irradiance, which facilitated a more accurate simulation of mixed layer temperature in a separate physical study. The productivity data presented here were incorporated into a carbon budget of the mixed layer, which derived a gas transfer velocity in excellent agreement with direct CO_2 flux measurements. *INDEX TERMS:* 4805 Oceanography: Biological and Chemical: Biogeochemical cycles (1615); 4806 Oceanography: Biological and Chemical: Carbon cycling; 4845 Oceanography: Biological and Chemical: Nutrients and nutrient cycling; 4853 Oceanography: Biological and Chemical: Photosynthesis; *KEYWORDS:* equatorial Pacific, primary productivity, carbon budget

Citation: Strutton, P. G., F. P. Chavez, R. C. Dugdale, and V. Hogue (2004), Primary productivity in the central equatorial Pacific (3°S 130°W) during GasEx-2001, *J. Geophys. Res.*, *109*, C08S06, doi:10.1029/2003JC001790.

1. Introduction

[2] The GasEx-2001 cruise was conducted in the vicinity of 3°S, 130°W, just south of the equatorial Pacific upwelling plume, in February 2001. The aim of this process study was to quantify and understand air-sea CO_2 flux in a region that is a strong CO_2 source to the atmosphere. A previous experiment, GasEx-98 [*McGillis et al.*, 2001], was performed in a CO_2 sink region in the eastern north Atlantic. The broader aim of this program is to obtain a greater understanding of air-sea gas exchange by comparing these two studies. The measurements and analyses aimed specifically at quantifying the surface exchange processes are described in several papers elsewhere in this special section [*McGillis et al.*, 2004]. The purpose of this contribution is to describe and explain the biological measurements from the upper water column. These results are then developed further into an upper water column carbon budget by *Sabine et al.* [2004].

[3] The physical, chemical, and biological processes in the equatorial Pacific are becoming relatively well understood, as a result of the U.S. JGOFS EqPac program [*Murray et al.*, 1995], the development of the Tropical Atmosphere Ocean (TAO) Array [*McPhaden et al.*, 1998], and the work of many other groups, as summarized by *LeBorgne et al.* [2002]. In the eastern and central equatorial Pacific, upwelling is generated by the trade winds, which generally blow from east to west and drive a maximum climatological upwelling velocity of ~3.5 m d^{-1} in the central Pacific [~150°W; *Chai et al.*, 1996]. During El Niño events, which occur every 3 to 7 years [*Quinn et al.*, 1987], this upwelling is weakened, or in extreme events, shut down completely [*McPhaden*, 1999], with dramatic effects on the

[1]Now at College of Oceanic and Atmospheric Sciences, Oregon State University, Corvallis, Oregon, USA.

0148-0227/04/2003JC001790$09.00

biological productivity of the region (again, see *LeBorgne et al.* [2002] for a summary). The upwelled waters are sourced from approximately the same depth as the equatorial undercurrent (EUC) core, so the chemical composition of the EUC largely determines the biological response to upwelling [*Dugdale et al.*, 2002].

[4] The ratio of iron to nitrate and carbon in the EUC is low [*Coale et al.*, 1996], as is the ratio of silicate to nitrate, assuring silicon limitation of diatom growth [*Ku et al.*, 1995]. Co-limitation of silicate uptake by silicate and iron concentrations has been shown in diatom cultures [*Leynaert et al.*, 2003]. Within the narrow (1°N to 1°S) upwelling area, modeling studies [*Chai et al.*, 2002] indicate that the ecosystem functions in a chemostat mode, in which the loss rates determine phytoplankton growth rates, and consequently the concentration of the limiting nutrient necessary to sustain these loss rates. The major loss rate is the grazing by zooplankton [*Frost and Franzen*, 1992], which results in recycling of the nitrogen, a low *f* ratio, and low new production [*Dugdale and Goering*, 1967; *Dugdale et al.*, 1992; *Wilkerson and Dugdale*, 1992]. Phytoplankton growth rates are equal to the grazing rates, and no blooms can occur under these conditions. Diatoms, which can sink more rapidly than the small picoplankton but are a small part of the phytoplankton, account for most of the sinking losses to be made up by nitrate (new nutrient) uptake. Since the sinking losses are small, the demand on nitrate is low, and most of the phytoplankton community's nitrogen demand is accounted for by ammonium, the regenerated form of nitrogen.

[5] Since the demand for nitrate is relatively low, it remains in the euphotic zone to be advected to the south and north of the equator. Similarly, the biological utilization of dissolved inorganic carbon (DIC) is incomplete, thereby generating the positive air-sea gradient in CO_2 and the strong flux of CO_2 to the atmosphere [*Feely et al.*, 1999]. As upwelled water with unused nutrients is advected away from the upwelling source, the major change that occurs in a region such as that studied by GasEx-2001 is that the loss rates are reduced only slightly by the lack of dilution by upwelling, and the ecosystem should be expected to continue functioning as on the equator. However, progressive losses will occur for both the macronutrients and iron, such that decreases in phytoplankton rates can be expected until nutrients are essentially exhausted at some distance from the equator.

[6] The details of the upper water column sampling program are described in detail below and elsewhere [*Johnson et al.*, 2004; *Sabine et al.*, 2004]. This paper describes the biological measurements (chlorophyll concentration, primary productivity, new production, and Fast Repetition Rate Fluorometry (FRRF)) and explains the variability observed within the context of the physical and chemical measurements. Using the productivity data in conjunction with measurements of DIC, pCO_2, and upper water column physics, *Sabine et al.* [2004] derived pCO_2 flux estimates and a gas transfer velocity that agreed very closely with the physical measurements [*McGillis et al.*, 2004]. The quality of this agreement validates this approach of combining the upper water column measurements with a primarily surface/atmospheric program, and further confirms the accuracy of the estimates obtained by the core GasEx-2001 groups.

2. Methods

2.1. Location of Data Collection

[7] The data presented here represent a subset of 51 hydrocast stations occupied between 5 February 2001 (year day (YD) 36) and 3 March 2001 (YD 62) aboard the NOAA vessel *Ronald H. Brown*. These stations were mostly located in the vicinity of the GasEx-2001 instrument array, as it drifted from approximately 3°S, 125°W to 2.3°S, 131.4°W [*Johnson et al.*, 2004]. A station was performed at noon almost every day. Figure 1 of *Johnson et al.* [2004] also shows the location of two "butterfly" surveys and two 24-hour intensive surveys (hydrocast every 3 hours) for which stations were performed at times other than local noon. Figure 1 shows the 17 stations that form the basis of the analysis presented here, plotted with a compilation of SeaWiFS chlorophyll daily images spanning YD 44 to 60. The SeaWiFS data have been spatially transformed to account for the westward Lagrangian movement of the GasEx-2001 study site, so that the tropical instability wave (TIW) feature is coherent and can be clearly seen.

2.2. CTD Sampling Depths

[8] Water samples were drawn from conductivity-temperature-depth (CTD) rosette bottles fired at depths corresponding to 100, 50, 30, 15, 5, 1, and 0.1% of surface light, plus a bottle at 200 m. The 0.1% light level ranged from 100 to 150 m, mean = 118 m. The majority of the CTD stations were performed at local noon, and the light% depths for sampling were determined from optical profiles (using a Satlantic Inc. SeaWiFS Profiling Multispectral Radiometer (SPMR)) performed immediately prior to the CTD cast at the same location. For stations not performed near local noon, the sampling depths were determined from the most recent optical profile. The SPMR consists of both a profiling package and a surface reference sensor, and measures downwelling irradiance and upwelling radiance at 13 wavelengths (10-nm bands) from 412 nm to 780 nm. It therefore accurately quantifies the spectral attenuation of photosynthetically available radiation (PAR: 400 nm to 700 nm). During processing of the productivity data, the sampling depths were adjusted using the pigment profile (chlorophyll + phaeopigments) and an algorithm based on work by *Morel* [1988]. These depths were used to calculate integrated (mgC or mmolC m^{-2} d^{-1}) and mean (mgC or mmolC m^{-3} d^{-1}) productivity over the mixed layer and to the 0.1% light level. Here the focus is primarily on the mean mixed layer properties, since the goal is to constrain the mixed layer carbon budget.

2.3. Chlorophyll Profiles

[9] Water samples of 500 mL were taken from a minimum of eight depths between 0 and 200 m and filtered at a vacuum pressure of <20 kPa onto Whatman 25-mm-diameter GFF filters. Samples were then extracted in 90% acetone at −10°C for a minimum of 24 hours, before determination of chlorophyll *a* and phaeopigments was performed in a Turner Designs model 10-005R benchtop fluorometer [*Holm-Hansen et al.*, 1965; *Lorenzen*, 1966]. The fluo-

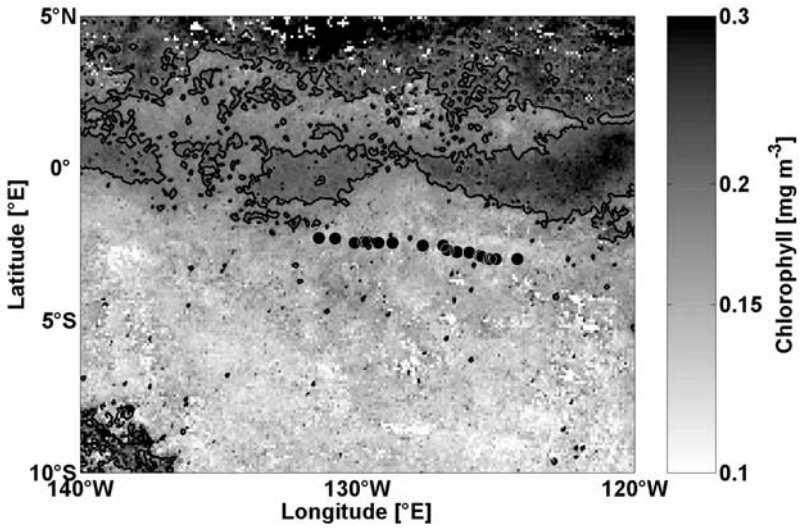

Figure 1. Daily SeaWiFS images from 13 February 2001 to 1 March 2001 (YD 44 to 60) mapped relative to the tracked parcel of water and averaged. The locations of the 17 CTD stations are also plotted. The progression of stations was generally from east to west. Chlorophyll concentrations are in mg m^{-3}, and the 0.2 mg m^{-3} contour is plotted.

rometer had been calibrated using known concentrations of chlorophyll *a* (Sigma chemicals), and this method is identical to that used by *Chavez et al.* [1996].

2.4. Primary Productivity

[10] In order to minimize the effects of metal contamination or chemical toxicity, the metallic springs and neoprene O-rings in the CTD rosette bottles were replaced with silicone rubber components for the duration of these cruises. In addition, a bottle-washing protocol based on that of *Fitzwater et al.* [1982] was employed at the beginning of the cruise.

[11] For each primary productivity profile, 280-mL water samples were taken from the 100 to 0.1% light depths described above, in polycarbonate bottles that had been washed using a similar procedure as for the CTD rosette bottles. One additional 280-mL sample each was drawn from the 100 and 0.1% depths for determination of the initial isotope uptake, subsequently referred to as the T_0 samples. To each of the 280 mL samples, 0.1 mL of $NaH^{14}CO_3$ (activity 0.1 mCi mL^{-1}) was added. The two T_0 samples were filtered immediately onto Whatman 25-mm-diameter GFF filters at a vacuum pressure of <20 kPa. The filters were then placed in 20-mL scintillation vials (Fisher Scientific) with 1 mL of ~0.5 N HCl (Fisher Scientific, reagent grade) and left uncapped for a minimum of 24 hours to drive off any abiotic $H^{14}CO_3$. The remaining samples were incubated on deck with running sea surface water in tubes fitted (or not in the case of the 100% samples) with screens designed to reduce the incident light to the levels at which the samples originated.

[12] After 24 hours, samples were removed, filtered at a vacuum pressure of <20 kPa onto Whatmann 25-mm GFF filters, and acidified as for the T_0 samples. After a minimum 24 hours, 10 mL of Cytoscint ES liquid scintillation cocktail was added to each of the acidified samples. Prior to filtering, 1 mL was extracted from the 100 and 0.1% samples and combined with 20 mL of Cytoscint ES (ICN Biomedicals) in a scintillation vial that was immediately capped; this was done in order to determine the total activity of the isotope initially added. All vials were shaken vigorously and, after a period of 24 hours or more, were analyzed in a Beckman liquid scintillation counter to determine ^{14}C activity, from which primary productivity at each depth was calculated as

$$\mathrm{CU} = \frac{(\mathrm{DPM_t} - \mathrm{DPM_0})\mathrm{TIC}}{\mathrm{DPM_{total}}\nu t}, \qquad (1)$$

where CU is carbon uptake in mmolC m^{-3} d^{-1}, DPM_t and DPM_0 are the activities of the samples at 24 and 0 hours, respectively, TIC is the concentration of total inorganic carbon (constant value of 2000 mmolC m^{-3} was used), DPM_{total} is the activity of the "total activity" samples, ν is the volume filtered (280 mL), and t is the incubation time, in days.

[13] The ^{14}C measurements obtained via this incubation method include both photosynthesis and respiration, so the results may be affected by the time of day that the incubations were started. That is, incubations begun at local dawn would include 12 hours of photosynthesis, followed by 12 hours of respiration. During darkness (respiration), some of the ^{14}C taken up during daylight should be respired into solution, and so not appear in the particulate fraction during filtration at the end of the incubation. By this reasoning, incubations begun at local dawn would most closely approximate net primary productivity, while incubations begun at local sunset would most closely approximate gross primary productivity. Incubations begun at local noon might fall in between these two estimates (where gross is greater than net). This pattern was indeed observed when integrated primary productivity was plotted as a function of local time for the two 24-hour intensive experiments (data not shown). However, the difference between local noon and local dawn stations was less than the accuracy of the method (~10%). For the analysis presented here, stations performed between ~0600 and ~1400 local

time are treated as accurately quantifying net primary productivity.

2.5. New Production

[14] Daily incubations using $^{15}NO_3$ and $^{15}NH_4$ were performed in order to partition the nitrogen uptake of the phytoplankton community into "new" and "recycled" pathways, respectively. Only the $^{15}NO_3$ data are reported here. Water samples (1.17-L polycarbonate bottles, cleaned using the same methods as for the CTD rosette bottles and ^{14}C incubation bottles) were drawn from the 100, 50, 30, 15, 5, and 1% light levels, that is, the same depths used for the ^{14}C incubations, excluding the 0.1% light depth. Trace amounts of approximately 10% ambient NO_3 or NH_4 concentration using $K^{15}NO_3$ or $^{15}NH_4Cl$ (99 at $\%^{15}N$, Cambridge Isotope Laboratories) were added, and the bottles placed in bags constructed from layers of window screen designed to simulate the appropriate light levels. These bags were placed in an on-deck Plexiglas incubator and cooled by flowing surface seawater for 24 hours. The samples were then filtered at a vacuum pressure of <20 kPa onto combusted (450°C for 12 hours) Whatmann 25-mm GFF filters. Frozen filters were transported to the laboratory and then dried (<60°C for >24 hours) and analyzed for ^{15}N enrichment with a Europa Scientific Roboprep-Tracermass mass spectrometer system [*Wilkerson and Dugdale*, 1992]. New production (the amount of primary productivity attributed to uptake of NO_3) and the *f* ratio (the ratio of new production to total primary production) were calculated according to *Dugdale and Wilkerson* [1986]. Briefly, the uptake rate, V_t [hr^{-1}], is given by

$$V_t = \frac{^{15}N_{xs}}{(^{15}N_{enr} - \langle F \rangle) \times T}, \quad (2)$$

where $^{15}N_{xs}$ is the atom% excess ^{15}N in the sample, $^{15}N_{enr}$ is the atom% ^{15}N in the initially labeled fraction, $\langle F \rangle$ is the naturally occurring abundance of ^{15}N, and T is the incubation time. The *f* ratio is then given by

$$f = \frac{V_t \times PON \times 24 \times 6.6}{PP}, \quad (3)$$

where PON is the particulate organic nitrogen (mmol m^{-3}) in the sample, and PP is primary productivity (mmol C m^{-3} d^{-1}). The factors 24 and 6.6 convert the nitrogen uptake from mmol N m^{-3} hr^{-1} to mmol C m^{-3} d^{-1} (6.6 is the Redfield ratio of C to N uptake).

2.6. Fast Repetition Rate Fluorometry

[15] A Fast Repetition Rate Fluorometer (FRRF: Chelsea FASTtracka) was used throughout the experiment in two different modes: profiling and underway. For profiling, the instrument was attached to the CTD rosette frame in place of the 24th bottle, with the optical end of the instrument uppermost. The instrument's gain was fixed at 64, and each flash sequence consisted of 100 excitation flashlets followed by 20 relaxation flashlets. Both the light and dark chambers were used, and 10 flash sequences were internally averaged per channel, per acquisition. The time between acquisitions was ~1 s, which at the typical rate of descent provided approximately one data point per meter in the vertical. After each CTD profile, the FRRF data were downloaded from the instrument and aligned with the profile and bottle data from the CTD package using the depth data from the FRRF's pressure sensor. In underway mode, the same flash sequence protocol was used, but with only the dark channel active, since it was the channel connected to the ship's underway flow. Ten flash sequences were averaged per acquisition, but the sleep time between acquisitions was adjusted to provide approximately one data point per minute. Data were downloaded at least once daily, and merged with the ship's underway data (position, temperature, salinity, etc.) using the FRRF's internal clock.

[16] The FRRF data were processed using the manufacturer's software: FRS v1.4. The main parameter of interest here is the photochemical quantum efficiency of photosynthesis (F_v/F_m, dimensionless). This parameter can be thought of as an indicator of the percentage of operational photosynthetic reaction centers, and thus perhaps photosynthetic rate.

2.7. Calculation of Mixed Layer Radiant Heating Rates

[17] In order to facilitate accurate modeling of the mixed layer heat budget [*Johnson et al.*, 2004], the chlorophyll profiles collected in the vicinity of the drifting instrument array were used to quantify radiant heating. Here radiant heating is defined as that part of the mixed layer heat budget due to the attenuation of incident solar irradiance by water and chlorophyll. For equatorial regions, *Schudlich and Price* [1992] used a Jerlov IB model that attenuates irradiance according to

$$I_Z = I_0 \times (I_1 \times \exp(-z/\lambda_1) + I_2 \times \exp(-z/\lambda_2)), \quad (4)$$

where I_Z is the shortwave irradiance at depth *z*, I_0 is the surface shortwave irradiance, I_1 and λ_1 are 0.6 and 1 m, respectively, accounting for the 60% of incident shortwave radiation that is attenuated in the upper 1 m of the water column (wavelengths >~700 nm), and I_2 and λ_2 are 0.4 and 17 m, respectively, accounting for wavelengths 400 nm $\leq \lambda_2 \leq$ 700 nm that are assumed to have a characteristic attenuation depth of 17 m. There are two potential problems with this parameterization. First, it assumes a constant mean chlorophyll concentration in the mixed layer. Second, as irradiance propagates down through the water column, the red wavelengths are attenuated more quickly than the blues and greens, so that to accurately quantify the propagation requires a spectral approach, rather than a bulk attenuation coefficient for that portion of the shortwave spectrum that penetrates below 1 m.

[18] Using the measured chlorophyll profiles interpolated at 1-m intervals, and a spectral propagation technique described by *Strutton and Chavez* [2004], the radiant heating of the mixed layer was determined for each CTD station. The calculations were forced using the integrated daily above-water shortwave radiation (I_0) measured from the ship's sensors for ±12-hour period from the time of the CTD. For convenience, the radiant heating rates were converted from °C s^{-1} to °C $month^{-1}$. These results were then compared with the Jerlov representation (equation (4)), as well as the parameterizations described by *Paulson and Simpson* [1981] and *Ohlmann* [2003]. The *Paulson and Simpson* [1981]

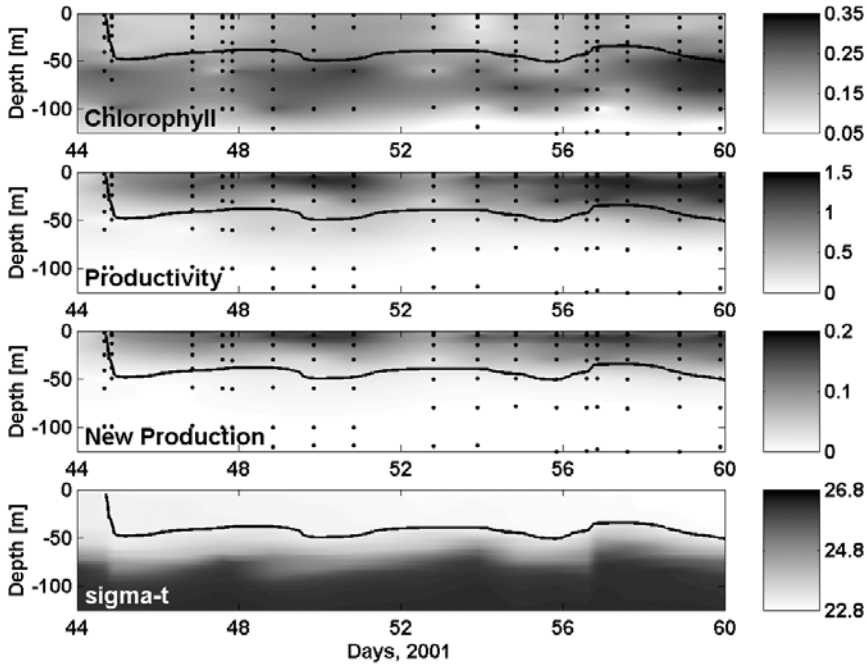

Figure 2. Time-depth plots of chlorophyll (mg m^{-3}), productivity (mmolC m^{-3} d^{-1}), new production (mmolC m^{-3} d^{-1}), and density excess (σ_t – kg m^{-3}), showing the vertical variability in biological and physical parameters during the course of the experiment. The contour in each plot is the 23.1 kg m^{-3} isopycnal, representing the base of the mixed layer.

method is essentially a Jerlov IB model, except that it partitions the incident light field into nine rather than two wavelength bands. The *Ohlmann* [2003] parameterization uses two wavelength bands as in equation (4), but the coefficients (I_1 and I_2) and exponents (λ_1 and λ_2) vary as a function of the local chlorophyll concentration.

2.8. Calculation of Integrated Quantities

[19] After experimenting with several different definitions for mixed layer depth, *Sabine et al.* [2004, Figure 5] used the 23.1 kg m^{-3} σ_t isopycnal as the base of the mixed layer. During the course of the experiment, mixed layer depth ranged from 30 to 51 m (mean 42 m). Integrated quantities such as chlorophyll, primary productivity, and new production were calculated by trapezoidal integration over the mixed layer based on the profile of discrete samples. Mean quantities were calculated using the discrete profile interpolated at 1-m intervals and then averaged, to avoid biasing of the mean because of non-uniform sampling depths in the mixed layer. Integrated and mean quantities were calculated over the mixed layer and not the euphotic zone because we are interested in the carbon budget of the former, not the latter.

3. Results

3.1. Temporal and Spatial Variability of Chlorophyll and Productivity

[20] Figure 1 provides an overview of the chlorophyll distributions in the vicinity of the GasEx-2001 experiment. The chlorophyll data are daily 9-km resolution, SeaWiFS Standard Mapped Images (SMIs). The equatorial upwelling plume was distorted by the passage of TIWs [*Legeckis*, 1977; *Halpern*, 1987; *Chelton et al.*, 2000], and the same pattern is visible in SST images [*Johnson et al.*, 2004]. In the context of the GasEx-2001 experiment it is sufficient to point out that the equatorial upwelling plume and the relatively high (up to 0.5 mg m^{-3}) surface chlorophyll concentrations associated with it were distorted into a wavelike structure of wavelength ~1000 km. Because the process study was carried out in a Lagrangian framework, the location of the instrument array and ship remained constant relative to the TIW structure. The daily SeaWiFS data in Figure 1 have been transposed to emphasize the TIW feature, but the station locations have not. That is, the measurements reported here were from a relatively low chlorophyll region (~0.1 to 0.15 mg m^{-3} surface chlorophyll, located at ~3°S, 128°W in Figure 1) bordered to the northeast and northwest by higher concentrations that had been advected southwards by the TIW currents.

[21] The 17 stations plotted in Figure 1 were chosen for the calculation of biological and chemical budgets from the total of 51 stations occupied. Stations were eliminated if they were performed before 0600 or after 1400 local time (see section 2.4), or away from the general drift path of the instrument array, such as the ''butterfly'' stations [see *Johnson et al.*, 2004, Figure 1]. Figure 2 shows the temporal variability in the vertical profiles of chlorophyll, primary productivity, new production, and density, based on these 17 stations. The depth-time plots have been overlaid with a contour at 23.1 kg m^{-3}, which was used as the definition of the base of the mixed layer [*Sabine et al.*, 2004]. The base of the region of elevated productivity closely follows the changes in the density profile, specifically shoaling of the pycnocline on days 44, 48, 54, and 57. Other features of note are a general increase in integrated primary productivity, caused mainly by an increase in the vertical extent of

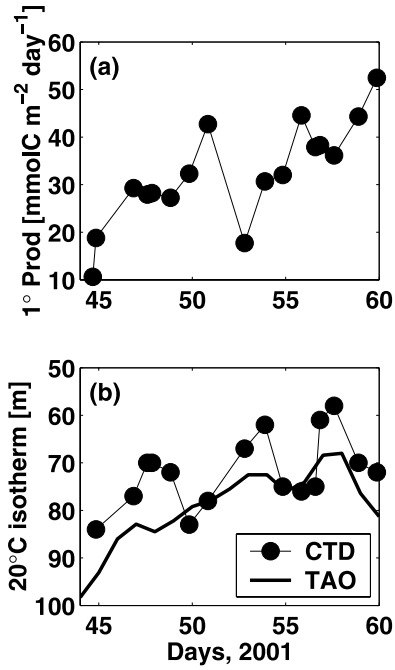

Figure 3. Time series of (a) integrated mixed layer primary productivity and (b) 20°C isotherm depth, a proxy for thermocline depth, calculated using both CTD profiles and the mean of the two closest TAO moorings located at 2°S 125°W and 2°S 140°W. The data clearly show a general increase in productivity during the course of the experiment, correlated with a shoaling of the thermocline. This shoaling has been attributed to the passage of a Kelvin wave [*Johnson et al.*, 2004].

the near-surface maximum in productivity. The station performed late on day 52 is an exception to this trend, because it was the first of the second butterfly CTD survey, and was slightly ahead of the Lagrangian trajectory of the experiment.

[22] The increase in integrated productivity was correlated with a shoaling of the thermocline. Figure 3 shows the time series of integrated mixed layer primary productivity, plotted with the time series of the depth of the 20°C isotherm ($Z_{20°C}$). $Z_{20°C}$ was determined from two data sets: (1) from the CTD temperature profiles, and (2) from the mean of the thermistor profiles from the two closest TAO moorings, located at 2°S 125°W and 2°S 140°W. $Z_{20°C}$ is routinely used as a proxy for the depth of the thermocline [*Chavez et al.*, 1998; *McPhaden*, 1999; *Turk et al.*, 2001; *Ryan et al.*, 2002], which in turn is an indicator of the proximity of nutrient source waters to the surface. The two methods for calculating $Z_{20°C}$ do not agree perfectly because (1) the two TAO moorings used are ~1600 km apart, and so incorporate some spatial variability, and (2) the vertical resolution of temperature sensors on the moorings is 25 m, versus 1-m averaged temperature data from the CTD. Figure 3 shows that integrated mixed layer primary productivity increased as the thermocline shoaled, due to the passage of an upwelling Kelvin wave [*Johnson et al.*, 2004].

[23] Figure 4 puts the changes in primary and new production in the context of the changes in dissolved inorganic carbon (DIC) and NO_3. Throughout the course of the experiment, a steady decrease in DIC (~11 μmol kg^{-1}) and NO_3 (~0.6 μmol kg^{-1}) occurred in conjunction with an increase in primary (~0.8 mmolC m^{-3} d^{-1}) and new production (~0.01 mmolN m^{-3} d^{-1}). *Sabine et al.* [2004] quoted a smaller value for the DIC decrease (6.5 μmol kg^{-1}) for a shorter time period (YD 47–60) than considered here (YD 44–60).

[24] On the basis of the 17 selected stations, the mean profiles of the relevant physical, biological, and chemical parameters were calculated and plotted in Figure 5. The nutricline (Figure 5b) is located immediately below the mixed layer (Figure 5a), where nitrate (silicate) concentrations increase by approximately 20 (15) μmol kg^{-1} over a vertical range of 40 m. The subsurface peak in chlorophyll (Figure 5c) corresponds with the location of the nutricline at around 60 m, but the maxima in primary productivity (Figure 5d) and new production (Figure 5e) are located at 5–10 m. The mean profile of the *f* ratio is also plotted (dashed line in Figure 5e), and shows a decrease from ~0.17 at the surface to ~0.04 at 60 m. The mean profile of F_v/F_m (Figure 5f) includes two subsurface maxima at approximately 25 m and 110 m. The relevance of these features is discussed below.

3.2. Fast Repetition Rate Fluorometry

[25] The underway F_v/F_m measurements show a declining trend during the transit to the experiment site (Figure 6a)

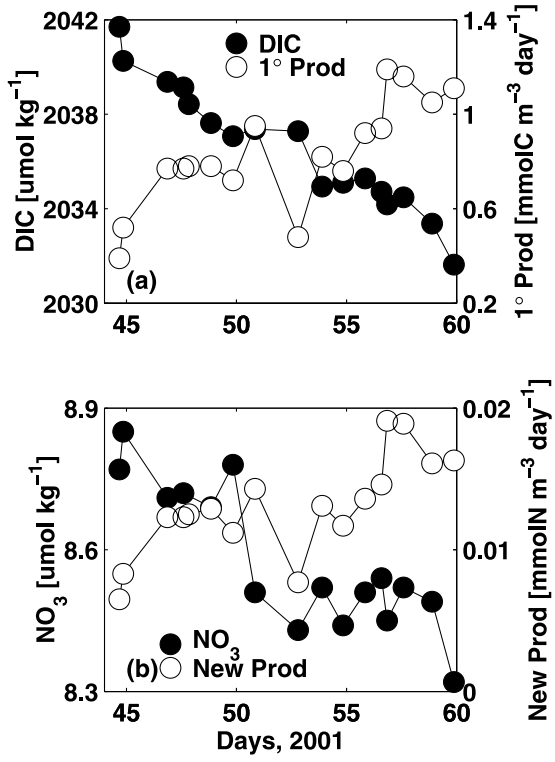

Figure 4. (a) Disappearance of dissolved inorganic carbon [μmol kg^{-1}] and increase in primary productivity (mmolC m^{-3} d^{-1}) throughout the course of the experiment. (b) Disappearance of nitrate (μmol kg^{-1}) and the increase in new production (mmolN m^{-3} d^{-1}) throughout the course of the experiment. All quantities are plotted as mixed layer means.

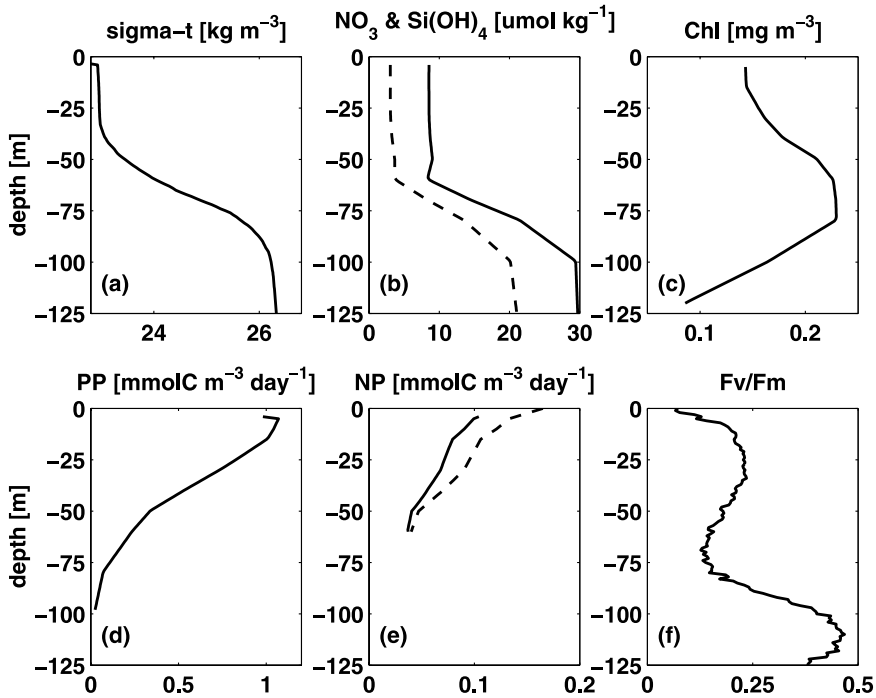

Figure 5. Mean profiles of (a) density excess (σ_t, kg m^{-3}), (b) nitrate (solid line) and silicate (dashed line) concentration (μmol kg^{-1}), (c) chlorophyll concentration (mg m^{-3}), (d) primary productivity (mmolC m^{-3} d^{-1}), (e) new production (solid line, mmolC m^{-3} d^{-1}) and the *f* ratio (dashed line, dimensionless), and (f) the photochemical quantum efficiency of photosynthesis (F_v/F_m, dimensionless) measured by the FRRF. All parameters plotted over the upper 125 m of the water column, and represent the mean profiles from 17 stations occupied during the central time period of the GasEx-2001 experiment (13 to 28 February 2001, YD 44 to 59).

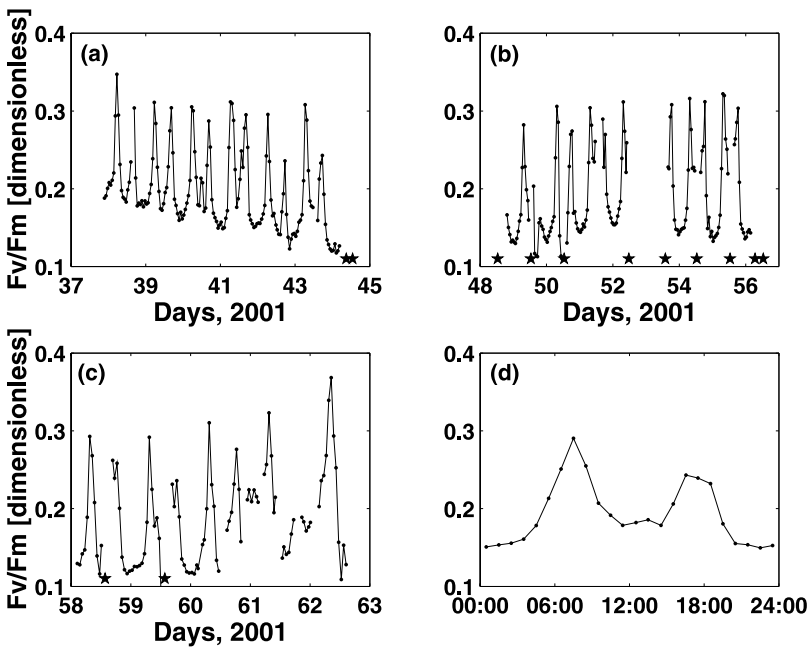

Figure 6. Underway measurements of the photochemical quantum efficiency of photosynthesis (F_v/F_m, dimensionless), made using the FRRF in flow-through mode. The data depicted are underway measurements made (a) during the transit to the GasEx-2001 study region, and (b, c) during the occupation of the study area. Timing of CTD stations is marked with pentagrams. (d) Mean daily cycle of F_v/F_m, plotted as a function of local time. Peaks are clearly observed at local sunrise and sunset, but interestingly, the pattern observed does not match either the iron replete or iron deficient cases observed by *Behrenfeld and Kolber* [1999].

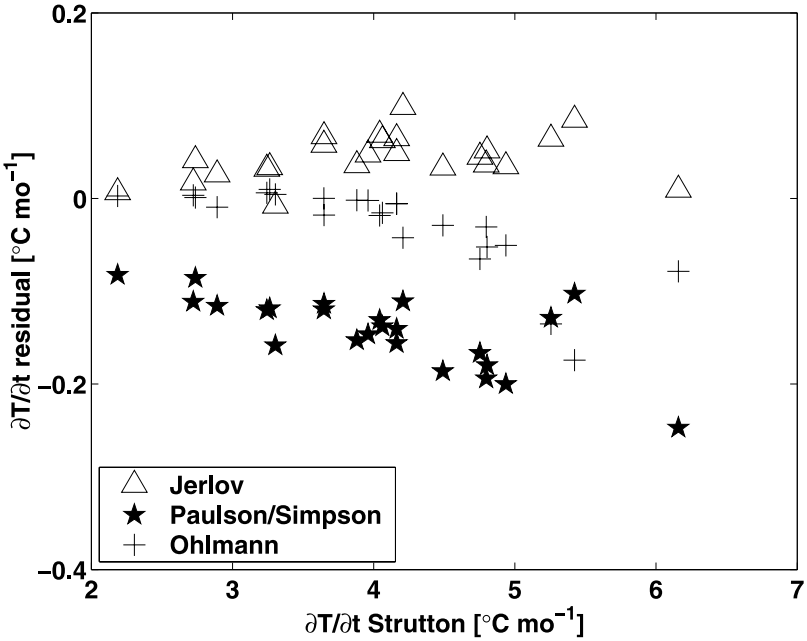

Figure 7. Comparison of methods for calculating the radiant heating of the mixed layer. Data are the residuals of each method calculated by subtracting the heating rate according to *Strutton and Chavez* [2004]. The mean heating rate for the data presented here was 4.03 ± 0.95°C month^{-1}. The Jerlov IB [*Schudlich and Price*, 1992] method tends to overestimate the heating rate at the higher end of the range, corresponding to shallower mixed layers, while the *Paulson and Simpson* [1981] method tends to underestimate heating because it is tuned to clear waters.

from 7 to 13 February 2001 (YD 38 to 44), with minimum daily values declining from approximately 0.2 to 0.12. In Figure 6b a slight increase in minimum daily values is observed, peaking around 21 February 2001 (YD 52), before the second butterfly survey began. During this period, maximum daily values varied very little, in contrast to the decline seen in Figure 6a. After 1 March 2001 (YD 60), when the ship began the transit to Hawaii through the equatorial upwelling plume, there is a discernable increase in daily maximum values, although the data are sparse due to the changing of the instrument between flow-through mode and profiling on the CTD (Figure 6c).

[26] Figure 6d shows the mean daily cycle of F_v/F_m based on the data in Figures 6a through 6c. Peaks are clearly visible at local sunrise and sunset, as was observed by *Behrenfeld and Kolber* [1999], but the magnitude of the local minimum near noon, attributed to photoinhibition, does not match their observations from the Pacific. It should be noted that *Behrenfeld and Kolber* [1999] normalized their mean daily cycle to the sunrise maximum each day. If the same normalization is performed on the data presented here (data not shown), there is no change in the overall pattern. The data were not normalized in Figure 6d so as to show the mean magnitude of the F_v/F_m measurements.

3.3. Radiant Heating

[27] The results of the radiant heating calculations are shown in Figure 7. The heating rate according to *Strutton and Chavez* [2004] is assumed to be the most accurate of the four methods used, because it uses the most detailed (yet computationally expensive) spectral attenuation model. The results of the Jerlov, Paulson, and Simpson and Ohlmann parameterizations are plotted as residuals ([method] − [Strutton method]), versus the calculated heating rate according to *Strutton and Chavez* [2004]. The data show that the Ohlmann method agrees very well with the Strutton method and the Jerlov model tends to overestimate radiant heating at the high end of the range, while the Paulson and Simpson method underestimates radiant heating, probably because of the large attenuation depths (corresponding to clear water) in the visible portion of the spectrum [see *Paulson and Simpson*, 1981, Table 1].

4. Discussion

4.1. Temporal and Spatial Variability of Chlorophyll and Productivity

[28] The GasEx-2001 study area was ~3°S, and therefore not in the region of strong upwelling that is focused on a narrow latitudinal band near the equator. The moderately high nutrient waters that are upwelled along the equator are advected north and south, a process that shapes the equatorial cool tongue. The bulk of the nutrient transport into the GasEx-2001 region therefore arrives horizontally, from the north or northeast, rather than via local upwelling. GasEx-2001 occurred during relatively strong equatorial upwelling and tropical instability wave (TIW) activity, and while the upper water column nitrate concentrations were not limiting, iron concentrations were presumably very low as a result of biological consumption at the equator. The water advected from the equator was low in silicate relative to nitrate (Figure 5b). The surface $Si(OH)_4$ concentrations for the duration of GasEx-2001

(mean = 3.1 μmol kg^{-1}) were close to the Ks values (1.57 to 2.42 μM) calculated by *Leynaert et al.* [2001]. It is precisely this co-limitation of primary production (i.e., DIC uptake) by iron and silicate that is responsible for the CO_2 surplus in surface waters and flux to the atmosphere [*Feely et al.*, 2002], a major factor in determining the location of the experiment.

[29] The general increase in productivity observed during the course of the experiment (Figures 2, 3, and 4) was correlated with a shoaling of the thermocline. Changes in thermocline depth have repeatedly been linked to changes in productivity [*Chavez et al.*, 1998; *Turk et al.*, 2001; *Ryan et al.*, 2002]; a shallower thermocline is usually associated with higher surface productivity. This occurs because, in the equatorial Pacific, the nitricline (and presumably the ferricline) corresponds with the thermocline; therefore shoaling of the thermocline brings the nutrient source closer to the surface, and upwelling or diffusion of nutrients into the euphotic zone then fuels enhanced productivity. Thermocline depth and productivity are not perfectly anti-correlated because of (among other factors) time delays in the phytoplankton response to thermocline variability.

[30] The vertical profiles of chemical and biological parameters are typical of the central and eastern equatorial Pacific [*Barber et al.*, 1996; *Chavez et al.*, 1996; *Strutton and Chavez*, 2000]. Nitrate (Figure 5b) is depleted to ~8 μM (not limiting), throughout the euphotic zone, and the nutricline corresponds with the thermocline. A subsurface chlorophyll maximum of ~0.2 mg m^{-3} is located at the nutricline (Figure 5c); this is a common feature of oligotrophic oceanic environments. *Parslow et al.* [2001] have recently described the processes potentially creating and maintaining such a subsurface maximum in an HNLC zone, while *Fennel and Boss* [2003] provided a mathematical description of subsurface chlorophyll and carbon maxima in oligotrophic regions. The productivity (Figure 5d) and F_v/F_m (Figure 5f) profiles show that the biomass located at 50 m to 75 m is not productive. The maximum in productivity (Figure 5d) just below the surface at 5 m to 15 m is largely driven by light; irradiance at the surface causes photoinhibition, which is also observed in the F_v/F_m profiles (Figure 5f). At 5 to 15 m, light levels are slightly decreased, so photoinhibition is relaxed, leading to higher productivity and F_v/F_m values. The deeper of the two subsurface F_v/F_m maxima is probably due to replete macronutrients (and possibly micronutrients) in the absence of any photoinhibition. This deeper max has little or no ecological significance since the biomass (Figure 5c) and light levels below 100 m are extremely low.

[31] The *f* ratio varied from 0.17 at the surface to 0.04 at 60 m, a range that is toward the low end of previous data from the equatorial Pacific under moderate upwelling conditions [*Dugdale et al.*, 1992; *McCarthy et al.*, 1996; *Aufdenkampe et al.*, 2001]. The decrease with depth occurs because NO_3 uptake is more strongly light dependent than NH_4 uptake over a 24-hour period. NO_3 uptake in the dark is miniscule, while nighttime NH_4 uptake is about half the daytime rate. Our samples were incubated at light levels ranging from 100% to 1% of surface irradiance. As light decreases, NO_3 uptake will decrease more rapidly as a function of depth than the corresponding NH_4 uptake, causing a decreasing *f* ratio with depth.

[32] Primary productivity levels were also a little below values previously measured. Figure 3 shows productivity integrated over the mixed layer ranging from 10 to 50 mmolC m^{-2} d^{-1}. The same data integrated to the 0.1% light level, so as to be consistent with previous work [*Barber et al.*, 1996; *Chavez et al.*, 1996; *Strutton and Chavez*, 2000] equate to a range of ~20 to 70 mmolC m^{-2} d^{-1} (compare the equatorial Pacific mean of 75 mmolC m^{-2} d^{-1}, or 900 mgC m^{-2} d^{-1} suggested by *Chavez et al.* [1996]). The GasEx-2001 rates are lower than average because the location of the measurements was away from the active upwelling zone. Measurements toward the beginning and end of the cruise, closer to or in the upwelling plume, reached 85 mmolC m^{-2} d^{-1} or greater. The mean *f* ratio profile, when applied to the primary productivity data, resulted in new production rates that decreased from ~0.15 mmolC m^{-3} d^{-1} near the surface to essentially zero at 60 m. The time series of integrated (and mean) mixed layer chlorophyll (data not shown) and new production (Figure 4b) both closely resemble the temporal variability in integrated productivity shown in Figures 3a and 4a. In the middle portion of the time series (~YD 50 to 55), there is a lag of approximately 1 day between changes in productivity and changes in chlorophyll, and Figure 2 shows that these increases are vertically decoupled; increases in productivity near the surface are associated with increases in chlorophyll around 60 m.

[33] The observed decreases in DIC and NO_3 agreed well with the measurements of primary production and new production. If we consider the 13-day period from year days 47 to 60 (to be consistent with *Sabine et al.* [2004]), mixed layer DIC decreased by 6.5 μmol kg^{-1}, while time-integrated primary production was 11.2 μmol kg^{-1}. The majority (69%) of this 6.5 μmol kg^{-1} decrease can be explained by air-sea gas exchange, which *Sabine et al.* [2004] calculated to be equivalent to a DIC decrease of 4.5 μmol kg^{-1}. Precipitation (dilution) and entrainment (enhancement) collectively contributed a net decrease of 0.9 μmol kg^{-1} DIC, 14% of the observed. Lateral diffusion and/or advection of DIC (and NO_3) were negligible because of the Lagrangian experimental setting [*Johnson et al.*, 2004; *Sabine et al.*, 2004]. The remaining 1.1 μmol kg^{-1} decrease in DIC was attributed to biological drawdown. This amount is far smaller than the observed time-integrated mean mixed layer primary productivity of 11.2 μmol kg^{-1} because the majority of the biologically fixed carbon is rapidly recycled. Note that biological DIC drawdown is 10% of the time-integrated primary productivity, which is equivalent to the nitrate-fueled proportion of total primary production. The measured mean mixed layer *f* ratio was 0.1, indicating that 90% of the primary productivity was fueled by ammonium uptake. The observed drawdown in NO_3 over days 47 to 60 was 0.24 μmol kg^{-1}, while time-integrated new production was 0.17 μmol kg^{-1}. Because NO_3 does not exchange with the atmosphere, as does CO_2, the percentage decrease in mixed layer NO_3 due to dilution and entrainment was 45% (0.11 μmol kg^{-1}), as opposed to 14% for DIC. This assumes that dilution and entrainment influenced NO_3 in the same way as DIC, and suggests that the actual time-integrated new production may be closer to 0.13 μmol kg^{-1} ($0.13_{\text{new production}}$ =

$0.24_{observed} - 0.11_{dilution/entrainment}$), rather than the measured 0.17 μmol kg^{-1}.

4.2. Nutrient Uptake Ratios

[34] Figure 4b shows the decrease in nitrate observed during the course of the experiment, and implies a rate of 0.023 μmol kg^{-1} d^{-1} (the slope of a linear fit to the data). The corresponding rates for silicate and phosphate were 0.019 and 0.003 μmol kg^{-1} d^{-1}, respectively, which equates to a NO_3:$Si(OH)_4$:PO_4 uptake ratio of 6.9:5.6:1. This assumes that dilution and entrainment affected all three nutrients equally. This differs from (1) Redfield (NO_3:$Si(OH)_4$:PO_4 ≈ 15:15:1), (2) in vitro measurements from *Takeda* [1998] for both ambient iron (NO_3:$Si(OH)_4$:PO_4 ≈ 23:30:1) and iron-replete (NO_3:$Si(OH)_4$:PO_4 ≈ 15:7:1) natural populations at 0° 159°W, and (3) in vitro measurements from *Hutchins et al.* [2002] for coastal iron-limited populations (NO_3:$Si(OH)_4$:PO_4 ≈ 7:15:1).

[35] To understand this NO_3:$Si(OH)_4$:PO_4 uptake ratio of 6.9:5.6:1, we break it down into two components. First, the uptake ratio for NO_3:$Si(OH)_4$) is close to 1:1, consistent with that reported by *Dugdale and Wilkerson* [1998], indicating that most of the nitrate uptake was due to diatoms, a conclusion reached by others in JGOFS investigations at the same location [*Landry et al.*, 1997]. Silicate uptake kinetics measured with the radio-isotope ^{32}Si [*Leynaert et al.*, 2001], when compared with iron-silicate co-limited kinetics of diatoms in culture [*Leynaert et al.*, 2003], suggest no Fe limitation of diatom nutrient uptake on the equator, probably the result of sufficient iron upwelled along with nutrients. The uptake ratios reported here are consistent with that interpretation. Second, the NO_3:PO_4 and $Si(OH)_4$:PO_4 uptake ratios are unusually low. We suggest this is due to the dominance of the smaller phytoplankton (i.e., non-diatom) size classes away from significant upwelling at the equator. These organisms are presumably fulfilling their N requirement from ammonium (NH_4), while also using PO_4, thereby increasing the uptake of PO_4 relative to NO_3 and $Si(OH)_4$.

[36] To put the uptake ratio calculations for GasEx-2001 in a broader context, calculations of nutrient uptake were also made using a database of CTD stations in the equatorial Pacific, spanning 1980 to the present. For these calculations it was assumed that the nutrient concentration some depth below the thermocline (200 m is used here) and the nutrient concentration at the surface (5 m) represent the minimum and maximum effects of biological uptake, respectively. The difference between the two values is then uptake, which can be used to derive a NO_3:$Si(OH)_4$:PO_4 uptake ratio. Figure 8a shows these uptake ratios as a function of latitude for all stations in the database between 125°W and 140°W. Applying this method to the GasEx-2001 data, only, results in a NO_3:$Si(OH)_4$:PO_4 uptake ratio of 15.5:14.6:1, which is roughly consistent with Figure 8a, indicating that the GasEx-2001 conditions were representative of the climatology.

[37] This method of calculating uptake should only accurately reflect local uptake rates at the equator, that is, directly above the source of the upwelled water. As this upwelled water is advected north and south from the equator, the uptake ratios calculated via vertical differencing at higher latitudes begin to reflect the local uptake processes.

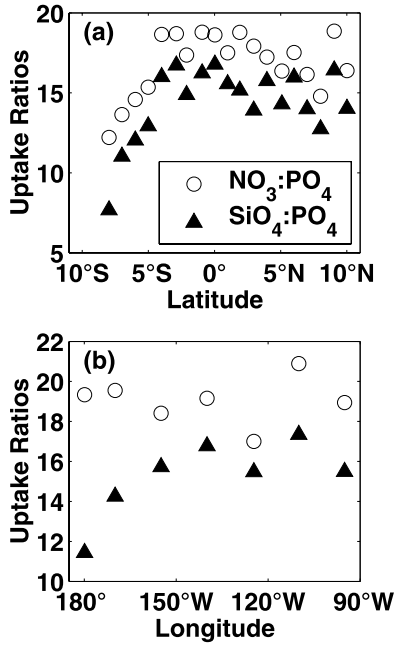

Figure 8. (a) Uptake ratio of nitrate and silicate relative to phosphate, derived from 340 CTD stations performed from 1980 onward, between 125°W and 140°W in the equatorial Pacific. (b) Same ratios plotted as a function of longitude, derived from 290 stations for the same time period, between 1°N and 1°S.

For example, the uptake ratio calculated only based on the disappearance of mixed layer nutrients from the GasEx-2001 nutrient time series was 6.9:5.6:1. The climatological value of 18.7:16.7:1 at 3°S in Figure 8a is essentially identical to the "time-zero" (equatorial) ratio of 18.6:16.8:1. South of 3°S the ratios rapidly decrease, which reflects the influence of the local uptake ratios on the ratios that are "exported" from the equator. A similar uptake plot (Figure 8b) as a function of longitude for all stations within 1° north and south of the equator shows that the uptake of $Si(OH)_4$ in particular decreases west of ~150°W, as the rate of upwelling dramatically declines [*Chai et al.*, 1996].

4.3. Fast Repetition Rate Fluorometry

[38] F_v/F_m measured by FRR fluorometry has been shown to vary considerably at daily timescales, and as a result of the nutrient status of phytoplankton. Empirical evidence suggests that F_v/F_m ranges from ~0.1 for nutrient- (usually iron-) stressed phytoplankton communities to a maximum of 0.65 for nutrient replete communities not experiencing photoinhibition [*Kolber and Falkowski*, 1993; *Behrenfeld et al.*, 1996; *Behrenfeld and Kolber*, 1999]. *Behrenfeld and Kolber* [1999] observed large nocturnal decreases in underway F_v/F_m in the south Pacific gyre (SPG) and the equatorial upwelling region (EU), and interpreted these fluctuations as being diagnostic of iron limitation. The GasEx-2001 underway FRRF data show a similar nighttime pattern. However, the secondary minima in F_v/F_m observed during the day, attributed by *Behrenfeld and Kolber* [1999] to photoinhibition, are more pronounced in the GasEx-2001 data [see *Behrenfeld and Kolber*, 1999, Figure 3a]. This is curious, since the data were collected in

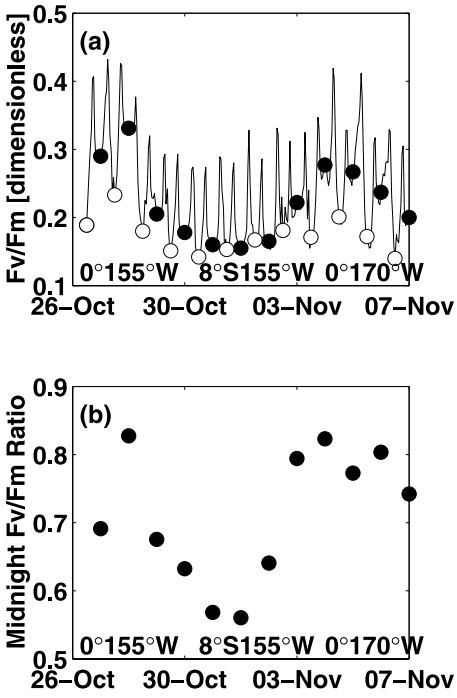

Figure 9. (a) Underway FRRF data from the equatorial Pacific, October–November 1999, a period of moderate to strong upwelling. The data displayed are along a cruise track from 0° 155°W to 8°S 155°W, then northwest to 0° 170°W. At the end of the record (~6 November 1999) the ship is heading south away from the equatorial upwelling tongue. Strong diurnal variability is visible in the F_v/F_m data; midnight readings are denoted by solid circles, and noon readings are denoted by open circles. (b) Decrease in F_v/F_m observed at midnight, expressed as a ratio to the mean of the neighboring sunset and sunrise values.

the same region, with presumably similar irradiance (i.e., photoinhibition) conditions. Closer comparison of the two data sets indicates that the difference in F_m between noon and midnight during GasEx-2001 was significantly less than for the *Behrenfeld and Kolber* [1999] data, therefore leading to a larger signal in F_v/F_m. The reason for this difference is not immediately apparent, but may be related to seasonal or interannual variability in phytoplankton physiology.

[39] To further investigate the *Behrenfeld and Kolber* [1999] diagnostic of iron limitation, underway FRRF data from a previous equatorial Pacific cruise are plotted in Figure 9a. These data were collected in October–November 1999, a period of moderate to strong upwelling, aboard the NOAA ship *Ka'imimoana*. The data displayed are hourly means along a cruise track from 0° 155°W to 8°S 155°W, then northwest to 0° 170°W and south to ~2°S 170°W. In relation to the upwelling plume, the data around 26 to 28 October 2002 and 4 to 6 November 2002 are close to the upwelling center and least likely to be nutrient limited, while the data in the middle and at the very end of the record are south of the upwelling in more nutrient-poor waters. In order to highlight the diurnal variability, midnight samples are plotted as solid circles, and noon values are plotted as open circles. The decrease in F_v/F_m at night is clearly evident, as is the strong photoinhibition during the day. The magnitude of the nighttime decrease in F_v/F_m was quantified by taking each midnight F_v/F_m value, and dividing it by the mean of the neighboring sunset and sunrise values; the results are plotted in Figure 9b. There is a clear decrease in the ratio, indicating a larger decrease in midnight F_v/F_m, in the regions distant from the upwelling center. Therefore, if the magnitude of the decrease in F_v/F_m can be considered a quantitative measure of the amount of iron limitation, the observed patterns concur with what is know about the distribution of iron in the equatorial Pacific. The same calculations were performed using the GasEx-2001 FRRF data (results not shown) and revealed a general increase in this "midnight F_v/F_m ratio" parameter corresponding with the shoaling of the thermocline (Figure 3b), indicating a slight relaxation of iron limitation during the experiment.

4.4. Radiant Heating

[40] As described above, calculations of radiant heating in the mixed layer using a Jerlov IB model with an attenuation depth of 17 m tended to overestimate radiant heating at the high end of the observed heating rates. In the same range, the *Ohlmann* [2003] parameterization only slightly underestimated heating, while the *Paulson and Simpson* [1981] method, tuned to clear waters, led to underestimates of up to 0.2°C month^{-1}. Figure 7 showed that the discrepancies with all three methods were greater at the higher end of the observations, which corresponds to shallow mixed layer depths. This emphasizes the point raised by *Strutton and Chavez* [2004], that sensitivity of the radiant heating calculation to chlorophyll concentration is greater for shallow mixed layers. Comparison with the results obtained using the measured chlorophyll profiles [*Morel and Maritorena*, 2001; *Strutton and Chavez*, 2004] suggested 25 m as a more accurate attenuation depth for the Jerlov IB model (i.e., a mean mixed layer chlorophyll concentration lower than that assumed in the original Jerlov parameterization). *Johnson et al.* [2004] subsequently incorporated this attenuation depth into their physical model [*Price et al.*, 1986] and found that the mixed layer temperature, which had previously been overestimated by ~0.4°C, now replicated the observed temperature variability almost exactly. This result underscores the potential importance of attenuation by phytoplankton in the heat budget of the mixed layer. For a mixed layer of 50 m, which corresponds to the maximum observed during GasEx-2001, *Strutton and Chavez* [2004] found that relatively minor fluctuations in mean mixed layer chlorophyll concentrations (from 0.1 to 0.3 mg m^{-3}) can lead to changes in the heat flux out of the mixed layer into the deeper ocean of ~5 W m^{-2}. This value is close to the changes in meridional heat flux associated with El Niño events described by *White et al.* [2001], which suggests that every effort should be made to include realistic radiant heating parameterizations in physical models of the equatorial Pacific.

5. Conclusions

[41] In this contribution we have quantified mixed layer primary productivity and new production during GasEx-2001, and compared these processes with FRRF data and mixed layer nutrient budgets. The results are consistent with moderate productivity in an iron-silicate co-limited

upwelling environment. Throughout the course of the experiment, mixed layer productivity increased from 10 to 50 mmolC m^{-2} d^{-1} owing to the passage of an upwelling Kelvin wave [*Johnson et al.*, 2004], which shoaled the thermocline by ~20 to 30 m. This increase in productivity was consistent with the results from underway fast repetition rate fluorometry (FRRF). In addition to the biological-physical coupling illustrated by the Kelvin wave—productivity relationship, our results also documented the importance of using biological data to accurately model the heat budget of the mixed layer.

[42] Within the larger scope of GasEx-2001, the purpose of the upper water column CTD-based measurements was to construct a carbon budget for the water parcel followed by the ship, and thereby determine the CO_2 flux to the atmosphere. These calculations are described by *Sabine et al.* [2004], and the results agree well with the CO_2 fluxes determined from the above-water measurements. With the exception of the iron fertilization experiments that have been performed since the early 1990s, few, if any, observational studies have followed a parcel of water for 2 weeks. For GasEx-2001, this opportunity enabled the validation of an above-water derived gas transfer velocity. Discrepancies remain between the observed and modeled transfer velocities [*Hare et al.*, 2004], but further analysis of the biological data in conjunction with the physics and chemistry may help to resolve these uncertainties.

[43] **Acknowledgments.** We thank James Smith and the crew of the NOAA vessel *Ronald H. Brown*, in particular Jonathan Shannahoff, for their excellent assistance at sea. Calvin Mordy, Marilyn Roberts, and Dana Greeley provided the nutrient and dissolved inorganic carbon data. Chris Sabine and Greg Johnson provided helpful discussions. Mooring data were obtained from the TAO Project (PMEL/NOAA). SeaWiFS chlorophyll data were obtained from the SeaWiFS Project and the Distributed Active Archive Center (DAAC) at the Goddard Space Flight Center, Greenbelt, Maryland, under NASA's Mission to Planet Earth Program. NOAA and the David and Lucile Packard Foundation provided financial support.

References

Aufdenkampe, A. K., J. J. McCarthy, M. Rodier, C. Navarette, J. Dunne, and J. W. Murray (2001), Estimation of new production in the tropical Pacific, *Global Biogeochem. Cycles*, *15*, 101–112.

Barber, R. T., M. P. Sanderson, S. T. Lindley, F. Chai, J. Newton, C. C. Trees, D. G. Foley, and F. P. Chavez (1996), Primary productivity and its regulation in the equatorial Pacific during and following the 1991–1992 El Niño, *Deep Sea Res., Part II*, *43*, 933–969.

Behrenfeld, M. J., and Z. S. Kolber (1999), Widespread iron limitation of phytoplankton in the South Pacific Ocean, *Science*, *283*, 840–843.

Behrenfeld, M. J., A. J. Bale, Z. S. Kolber, J. Aiken, and P. G. Falkowski (1996), Confirmation of iron limitation of phytoplankton photosynthesis in the equatorial Pacific Ocean, *Nature*, *383*, 508–511.

Chai, F., S. T. Lindley, and R. T. Barber (1996), Origin and maintenance of a high nitrate condition in the equatorial Pacific, *Deep Sea Res., Part II*, *43*, 1031–1064.

Chai, F., R. T. Barber, R. C. Dugdale, T.-H. Peng, and F. P. Wilkerson (2002), One dimensional ecosystem model of the equatorial Pacific upwelling system: 1. Model development and silicon and nitrogen cycle, *Deep Sea Res., Part II*, *49*, 2713–2745.

Chavez, F. P., K. R. Buck, S. K. Service, J. Newton, and R. T. Barber (1996), Phytoplankton variability in the eastern and central tropical Pacific, *Deep Sea Res., Part II*, *43*, 835–870.

Chavez, F. P., P. G. Strutton, and M. J. McPhaden (1998), Biological-physical coupling in the central equatorial Pacific during the onset of the 1997–1998 El Niño, *Geophys. Res. Lett.*, *25*, 3543–3546.

Chelton, D. B., F. J. Wentz, C. L. Gentemann, R. A. de Szoeke, and M. G. Schlax (2000), Satellite microwave SST observations of trans-equatorial tropical instability waves, *Geophys. Res. Lett.*, *27*, 1239–1242.

Coale, K. H., et al. (1996), A massive phytoplankton bloom induced by an ecosystem-scale iron fertilization experiment in the equatorial Pacific Ocean, *Nature*, *383*, 495–501.

Dugdale, R. C., and J. J. Goering (1967), Uptake of new and regenerated forms of nitrogen in primary productivity, *Limnol. Oceanogr.*, *12*, 196–206.

Dugdale, R. C., and F. P. Wilkerson (1986), The use of 15N to measure nitrogen uptake in eutrophic oceans: Experimental considerations, *Limnol. Oceanogr.*, *31*, 673–689.

Dugdale, R. C., and F. P. Wilkerson (1998), Silicate regulation of new production in the equatorial Pacific upwelling, *Nature*, *391*, 270–273.

Dugdale, R. C., F. P. Wilkerson, R. T. Barber, and F. P. Chavez (1992), Estimating new production in the equatorial Pacific Ocean at 150°W, *J. Geophys. Res.*, *97*, 681–686.

Dugdale, R. C., A. G. Wischmeyer, F. P. Wilkerson, R. T. Barber, F. Chai, M. S. Jiang, and T. H. Peng (2002), Meridional asymmetry of source nutrients to the equatorial Pacific upwelling ecosystem and its potential impact on ocean-atmosphere CO_2 flux: A data and modeling approach, *Deep Sea Res., Part II*, *49*, 2513–2531.

Feely, R. A., R. Wanninkhof, T. Takahashi, and P. Tans (1999), Influence of El Niño on the equatorial Pacific contribution to atmospheric CO_2 accumulation, *Nature*, *398*, 597–601.

Feely, R. A., et al. (2002), Seasonal and interannual variability of CO_2 in the equatorial Pacific, *Deep Sea Res., Part II*, *49*, 2443–2469.

Fennel, K., and E. Boss (2003), Subsurface maxima of phytoplankton and chlorophyll: Steady-state solutions from a simple model, *Limnol. Oceanogr.*, *48*, 1521–1534.

Fitzwater, S. E., G. A. Knauer, and J. H. Martin (1982), Metal contamination and its effects on primary production, *Limnol. Oceanogr.*, *27*, 544–551.

Frost, B. W., and N. C. Franzen (1992), Grazing and iron limitation in the control of phytoplankton stock and nutrient concentration: A chemostat analogue of the Pacific equatorial upwelling zone, *Mar. Ecol. Prog. Ser.*, *83*, 291–303.

Halpern, D. (1987), Observations of annual and El Niño thermal and flow variations at 0°, 110°W and 0°, 95°W during 1980–1985, *J. Geophys. Res.*, *92*, 8197–8212.

Hare, J. E., C. W. Fairall, W. R. McGillis, J. B. Edson, B. Ward, and R. Wanninkhof (2004), Evaluation of the National Oceanic and Atmospheric Administration/Coupled-Ocean Atmospheric Response Experiment (NOAA/COARE) air-sea gas transfer parameterization using GasEx data, *J. Geophys. Res.*, *109*, C08S11, doi:10.1029/2003JC001831, in press.

Holm-Hansen, O., C. J. Lorenzen, R. W. Holmes, and J. D. Strickland (1965), Fluorometric determination of chlorophyll, *J. Cons. Cons. Int. Explor. Mer.*, *30*, 3–15.

Hutchins, D. A., G. F. Firme, and K. W. Bruland (2002), The influence of iron on the biology and biogeochemistry of the California coastal upwelling area, *Eos Trans. AGU*, *83*(47), Fall Meet. Suppl., Abstract OS61D-10.

Johnson, G. C., C. L. Sabine, K. E. McTaggart, and J. M. Hummon (2004), Physical oceanographic conditions during GasEx-2001, *J. Geophys. Res.*, *109*, C08S04, doi:10.1029/2002JC001718, in press.

Kolber, Z. S., and P. G. Falkowski (1993), Use of active fluorescence to estimate phytoplankton photosynthesis in situ, *Limnol. Oceanogr.*, *38*, 1646–1665.

Ku, T.-L., S. Luo, M. Kusakabe, and J. K. B. Bishop (1995), ^{228}Ra-derived nutrient budgets in the upper equatorial Pacific and the role of "new" silicate in limiting productivity, *Deep Sea Res., Part II*, *42*, 479–497.

Landry, M. R., et al. (1997), Iron and grazing constraints on primary production in the central equatorial Pacific: An EqPac synthesis, *Limnol. Oceanogr.*, *42*, 405–418.

LeBorgne, R., R. A. Feely, and D. J. Mackey (2002), Carbon fluxes in the equatorial Pacific: A synthesis of the JGOFS programme, *Deep Sea Res., Part II*, *49*, 2425–2442.

Legeckis, R. (1977), Long waves in the eastern equatorial Pacific Ocean: A view from a geostationary satellite, *Science*, *197*, 1179–1181.

Leynaert, A., P. Tréguer, C. Lancelot, and M. Rodier (2001), Silicon limitation of biogenic silica production in the equatorial Pacific, *Deep Sea Res., Part I*, *48*, 639–660.

Leynaert, A., E. Bucciarelli, P. Claquin, R. C. Dugdale, V. Martin-Jezequel, P. Pondaven, and O. Ragueneau (2003), Effect of iron deficiency on diatom cell size and silicic acid uptake kinetics, *Limnol. Oceanogr.*, in press.

Lorenzen, C. J. (1966), A method for the continuous measurement of in vivo chlorophyll concentration, *Deep Sea Res.*, *13*, 223–227.

McCarthy, J. J., C. Garside, J. L. Nevins, and R. T. Barber (1996), New production along 140°W in the equatorial Pacific during and following the 1992 El Niño event, *Deep Sea Res., Part II*, *43*, 1065–1093.

McGillis, W. R., J. B. Edson, J. D. Ware, J. W. H. Dacey, J. E. Hare, C. W. Fairall, and R. Wanninkhof (2001), Carbon dioxide flux techniques performed during GasEx-98, *Mar. Chem.*, *75*, 267–280.

McGillis, W. R., et al. (2004), Air-sea CO_2 exchange in the equatorial Pacific, *J. Geophys. Res.*, *109*, C08S02, doi:10.1029/2003JC002256, in press.

McPhaden, M. J. (1999), Genesis and evolution of the 1997–98 El Niño, *Science*, *283*, 950–954.

McPhaden, M. J., et al. (1998), The tropical Ocean Global Atmosphere observing system: A decade of progress, *J. Geophys. Res.*, *103*, 14,169–14,240.

Morel, A. (1988), Optical modeling of the upper ocean in relation to its biogenous content (Case I Waters), *J. Geophys. Res.*, *93*, 10,749–10,768.

Morel, A., and S. Maritorena (2001), Bio-optical properties of oceanic waters: A reappraisal, *J. Geophys. Res.*, *106*, 7163–7180.

Murray, J. W., E. Johnson, and C. Garside (1995), A U.S. JGOFS Process Study in the equatorial Pacific (EqPac): Introduction, *Deep Sea Res., Part II*, *42*, 275–293.

Ohlmann, J. C. (2003), Ocean radiant heating in climate models, *J. Clim.*, *16*, 1337–1351.

Parslow, J. S., P. W. Boyd, S. R. Rintoul, and F. B. Griffiths (2001), A persistent subsurface chlorophyll maximum in the Interpolar Frontal Zone south of Australia: Seasonal progression and implications for phytoplankton-light-nutrient interactions, *J. Geophys. Res.*, *106*, 31,543–31,558.

Paulson, C. A., and J. J. Simpson (1981), The temperature difference across the cool skin of the ocean, *J. Geophys. Res.*, *86*, 11,044–11,054.

Price, J. F., R. A. Weller, and R. Pinkel (1986), Diurnal cycling: Observations and models of the upper ocean response to diurnal heating, cooling and wind mixing, *J. Geophys. Res.*, *91*, 8411–8427.

Quinn, W. H., V. T. Neal, and S. E. A. Mayolo (1987), El Niño occurrences over the past four and a half centuries, *J. Geophys. Res.*, *92*, 14,449–14,461.

Ryan, J. P., P. S. Polito, P. G. Strutton, and F. P. Chavez (2002), Unusual large-scale phytoplankton blooms in the equatorial Pacific, *Prog. Oceanogr.*, *55*, 263–285.

Sabine, C. L., R. A. Feely, G. C. Johnson, P. G. Strutton, M. F. Lamb, and K. E. McTaggart (2004), A mixed layer carbon budget for the GasEx-2001 experiment, *J. Geophys. Res.*, *109*, C08S05, doi:10.1029/2002JC001747, in press.

Schudlich, R. R., and J. F. Price (1992), Diurnal cycles of current, temperature and turbulent dissipation in a model of the equatorial upper ocean, *J. Geophys. Res.*, *97*, 5409–5422.

Strutton, P. G., and F. P. Chavez (2000), Primary productivity in the equatorial Pacific during the 1997–1998 El Niño, *J. Geophys. Res.*, *105*, 26,089–26,101.

Strutton, P. G., and F. P. Chavez (2004), Biological heating in the equatorial Pacific: Observed variability and potential for real-time calculation, *J. Clim.*, *17*, 1097–1109.

Takeda, S. (1998), Influence of iron availability on nutrient consumption ratio of diatoms in oceanic waters, *Nature*, *393*, 774–777.

Turk, D., M. J. McPhaden, A. J. Busalacchi, and M. R. Lewis (2001), Remotely sensed biological production in the equatorial Pacific, *Science*, *293*, 471–474.

White, W. B., D. R. Cayan, M. D. Dettinger, and G. Auad (2001), Sources of global warming in upper ocean temperature during El Niño, *J. Geophys. Res.*, *106*, 4349–4367.

Wilkerson, F. P., and R. C. Dugdale (1992), Measurements of nitrogen productivity in the equatorial Pacific, *J. Geophys. Res.*, *97*, 669–679.

F. P. Chavez, Monterey Bay Aquarium Research Institute, 7700 Sandholdt Road, Moss Landing, CA 95039, USA. (chfr@mbari.org)

R. C. Dugdale and V. Hogue, Romberg Tiburon Center, San Francisco State University, PO Box 855, Tiburon, CA 94920, USA. (rdugdale@sfsu.edu; vhogue@sfsu.edu)

P. G. Strutton, College of Oceanic and Atmospheric Sciences, Oregon State University, Corvallis, OR 97331, USA. (strutton@coas.oregonstate.edu)